Electronic supplementary information

Ionic co-crystals of enantiopure and racemic histidine with calcium halides

Oleksii Shemchuk[a], Lorenzo Degli Esposti[b], Fabrizia Grepioni[a], Dario Braga[a]

[a]*Dipartimento di Chimica "G. Ciamician", Università degli Studi di Bologna, via Selmi 2 - 40126 Bologna, Italy*

[b]*Institute of Science and Technology for Ceramics (ISTEC), National Research Council (CNR), Via Granarolo 64, 48018 Faenza (RA), Italy*

Contents **page**

ESI - 1: Crystal Structure details.

Table ESI-1. *Single crystal* data and details of measurements for histidine ICCs with calcium halides.

	$(L\text{-}His)_2 \cdot CaCl_2 \cdot 3H_2O$	**$(L\text{-}His)_2 \cdot CaBr_2 \cdot 3H_2O$**	**$(DL\text{-}His)_2 \cdot CaBr_2 \cdot 4H_2O$**	**$(L\text{-}His)_2 \cdot CaI_2 \cdot 3H_2O$**
Formula	$C_{12}H_{24}CaCl_2N_6O_7$	$C_{12}H_{24}Br_2CaN_6O_7$	$C_{12}H_{26}Br_2Ca_1N_6O_8$	$C_{12}H_{24}CaI_2N_6O_7$
Fw ($g*mol^{-1}$)	475.35	564.27	582.28	658.25
Cryst. System	Monoclinic	Monoclinic	Triclinic	Orthorhombic
Space group	C 2	C 2	P -1	C 2 2 21
Z	2	2	1	4
a (Å)	20.6509(11)	20.9187(19)	4.8911(6)	4.9123(6)
b (Å)	5.1087(3)	5.1257(5)	10.0848(12)	20.333(2)
c (Å)	10.7880(5)	11.1180(7)	11.8785(13)	23.505(3)
α (deg)	90	90	95.772(9)	90.00
β (deg)	114.287(4)	115.051(6)	96.250(9)	90.00
γ (deg)	90	90	103.656(10)	90.00
V ($Å^3$)	1037.40(10)	1079.96(16)	561.11(11)	2347.8(5)
D_{calc} (g/cm^3)	1.522	1.735	1.723	1.862
μ (mm^{-1})	0.606	4.035	3.889	2.939
Measd reflns	2328	2479	3874	3715
Indep reflns	1720	1649	2517	2389
R_1 [on F_0^2, $I>2\sigma(I)$]	0.0390	0.0499	0.0938	0.0698
wR_2 (all data)	0.1306	0.1184	0.2683	0.1058

ESI - 2: TGA analyses

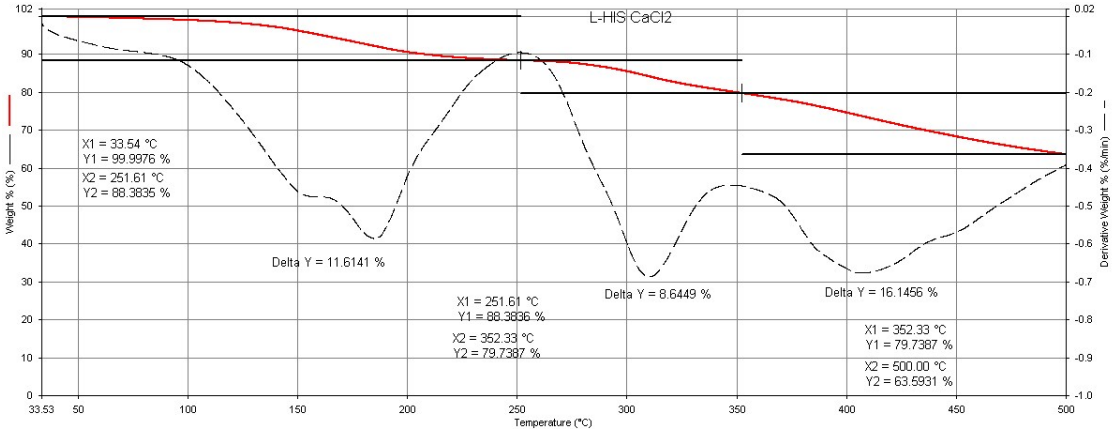

Figure ESI - 1. TGA trace for $(L\text{-}His)_2{\cdot}CaCl_2{\cdot}3H_2O$.

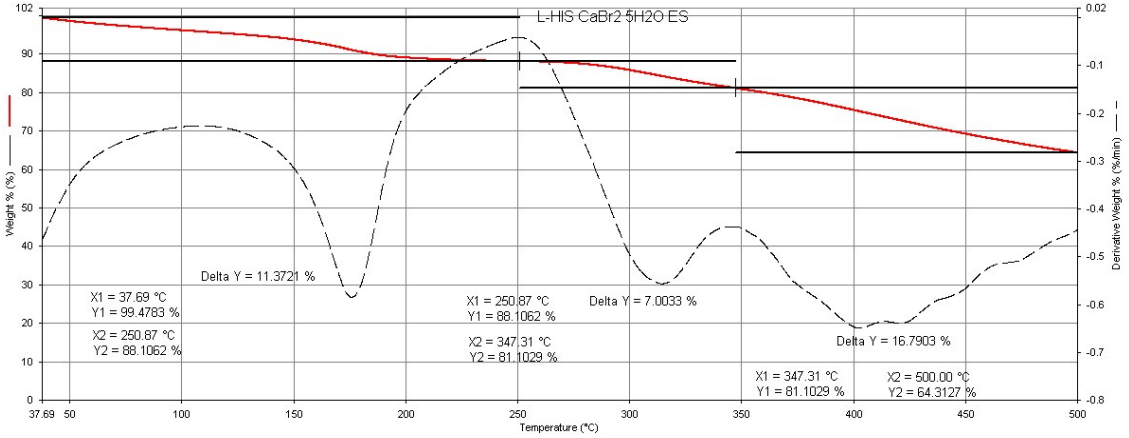

Figure ESI - 2. TGA trace for $(L\text{-}His)_2{\cdot}CaBr_2{\cdot}3H_2O$.

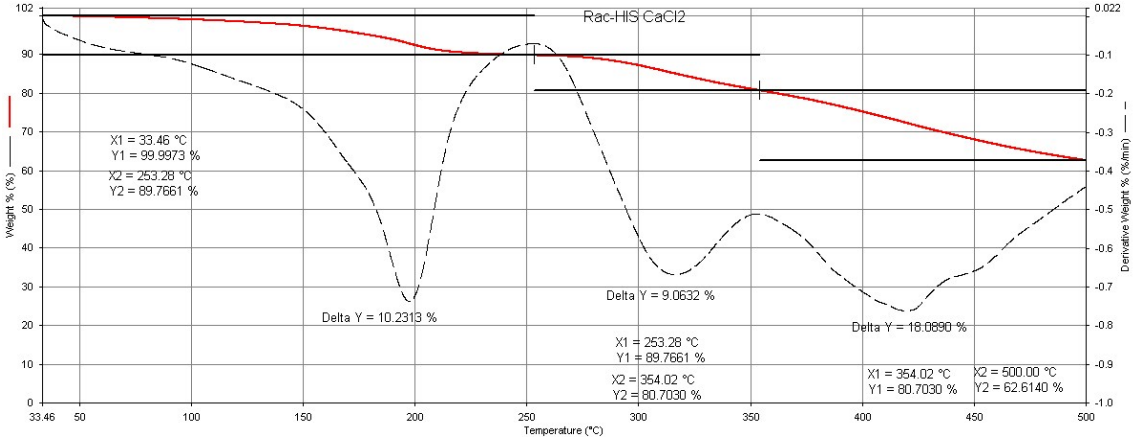

Figure ESI - 3. TGA trace for $(DL\text{-}His)_2{\cdot}CaCl_2{\cdot}3H_2O$.

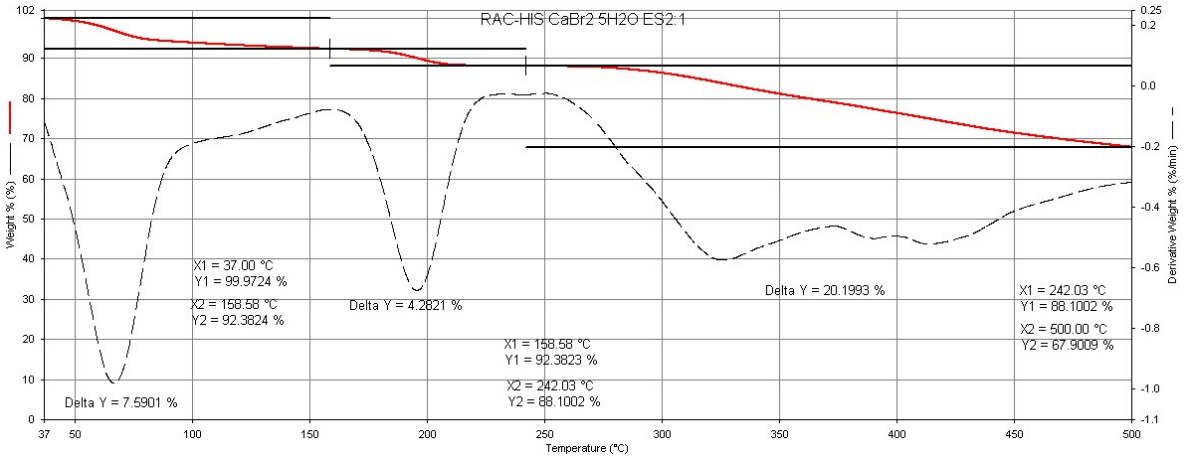

Figure ESI - 4. TGA trace for $(DL\text{-}His)_2{\cdot}CaBr_2{\cdot}4H_2O$.

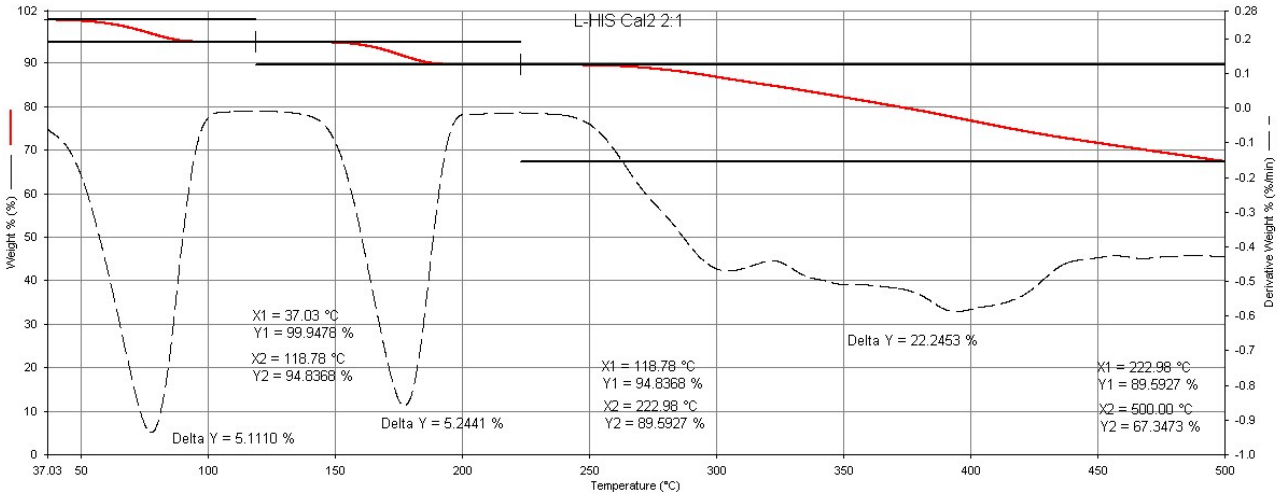

Figure ESI - 5. TGA trace for $(L\text{-}His)_2{\cdot}CaI_2{\cdot}4H_2O$.

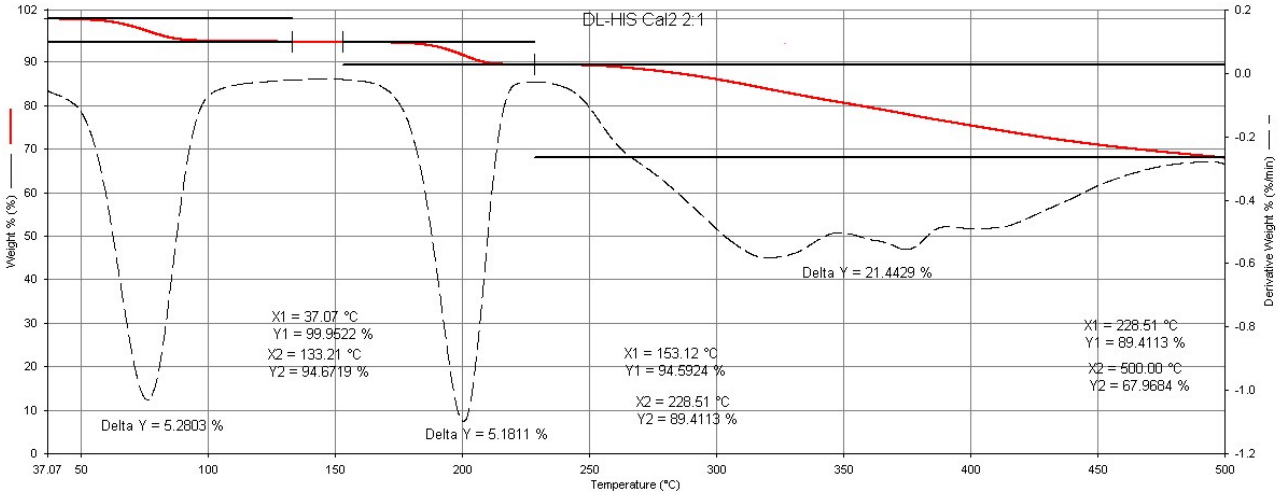

Figure ESI - 6. TGA trace for $(DL\text{-}His)_2{\cdot}CaI_2{\cdot}4H_2O$.

ESI - 3: Calculated and Experimental XRPD Patterns for $CaBr_2$ ICCs

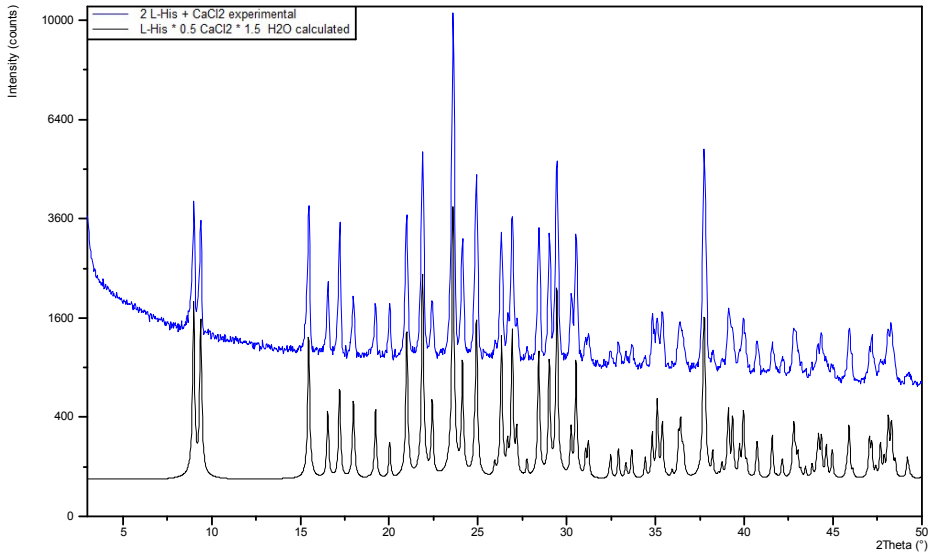

Figure ESI - 7. Comparison between the experimental (top) powder pattern of $(L\text{-}His)_2{\cdot}CaCl_2{\cdot}3H_2O$ and the one calculated (bottom) from single crystal data.

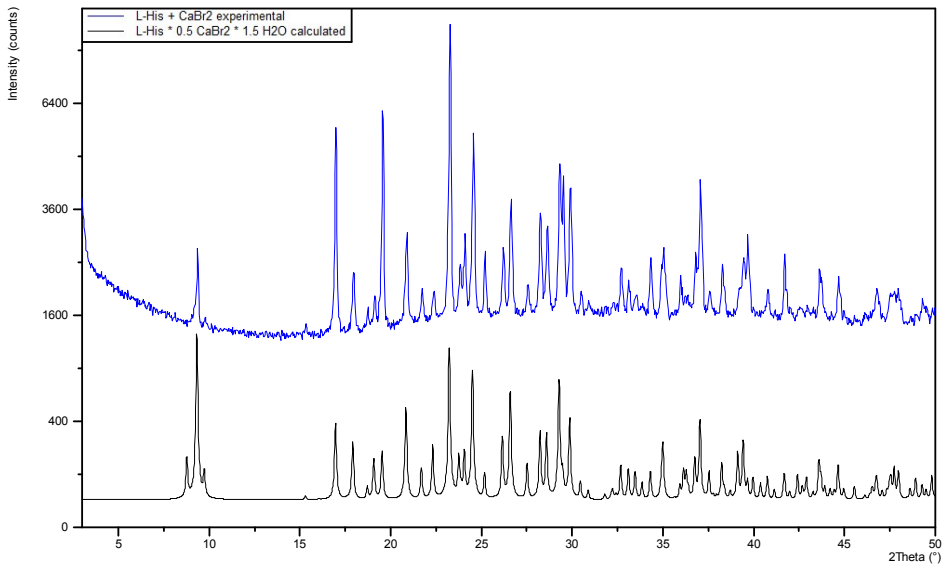

Figure ESI - 8. Comparison between the experimental (top) powder pattern of $(L\text{-}His)_2{\cdot}CaBr_2{\cdot}3H_2O$ and the one calculated (bottom) from single crystal data.

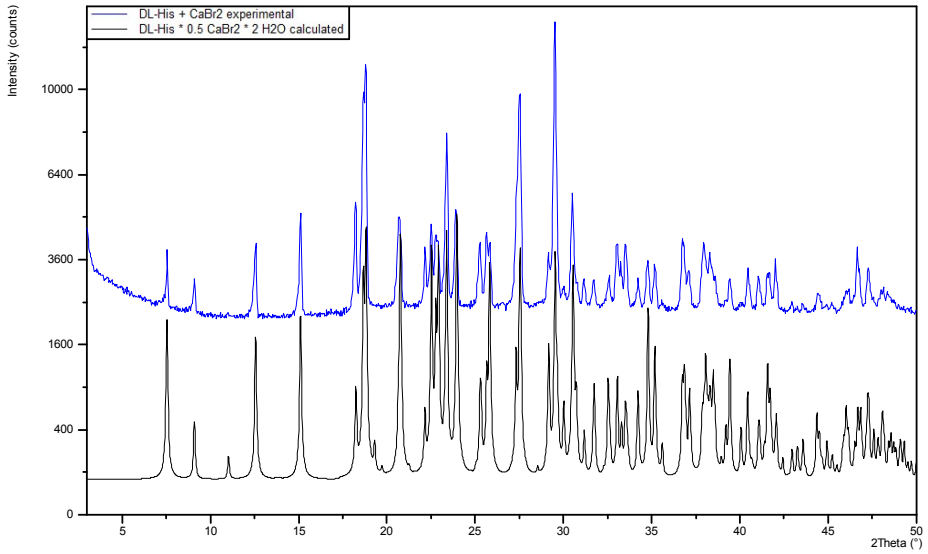

Figure ESI - 9. Comparison between the experimental (top) powder pattern of (DL-His)$_2$·CaBr$_2$·4H$_2$O and the one calculated (bottom) from single crystal data.

ESI - 4: Variable Temperature XRPD

Thermal programs for all samples are based on the thermogravimetric analysis profiles: first a pattern is collected at room temperature, then a program of stepwise heating (in the temperature range for which dehydration is observed in the TGA traces) is applied, followed by cooling to room temperature. Heating rate 30 °C min^{-1}. After each temperature has been reached, the sample is kept at that temperature for 5 min before an XRPD pattern is collected.

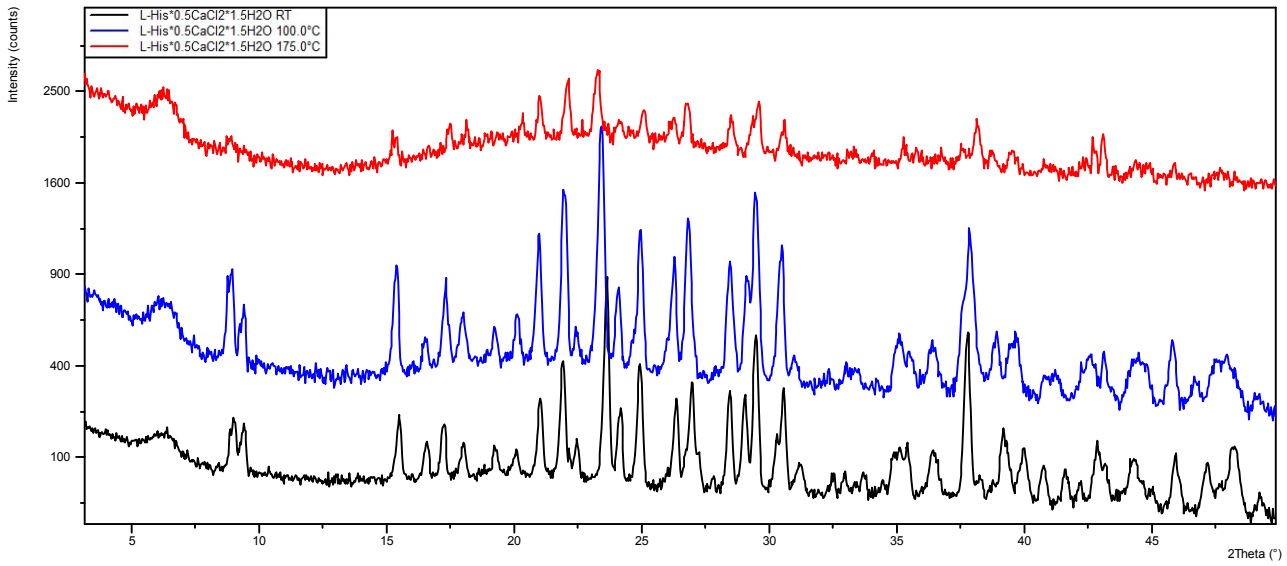

Figure ESI - 10. XRPD patterns of $(L\text{-}His)_2{\cdot}CaCl_2{\cdot}3H_2O$ at room temperature, 100 °C, 175 °C.

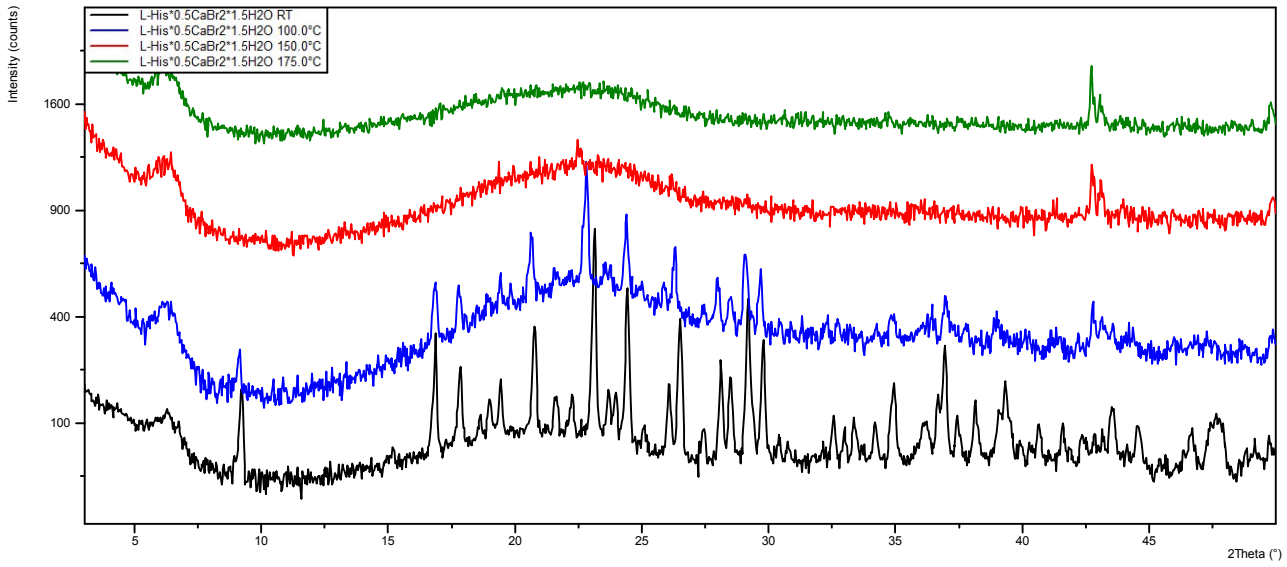

Figure ESI - 11. XRPD patterns of $(L\text{-}His)_2{\cdot}CaBr_2{\cdot}3H_2O$ at room temperature, 100°C, 150 °C, 175 °C. The peaks at 43 ° 2θ are due to the sample holder.

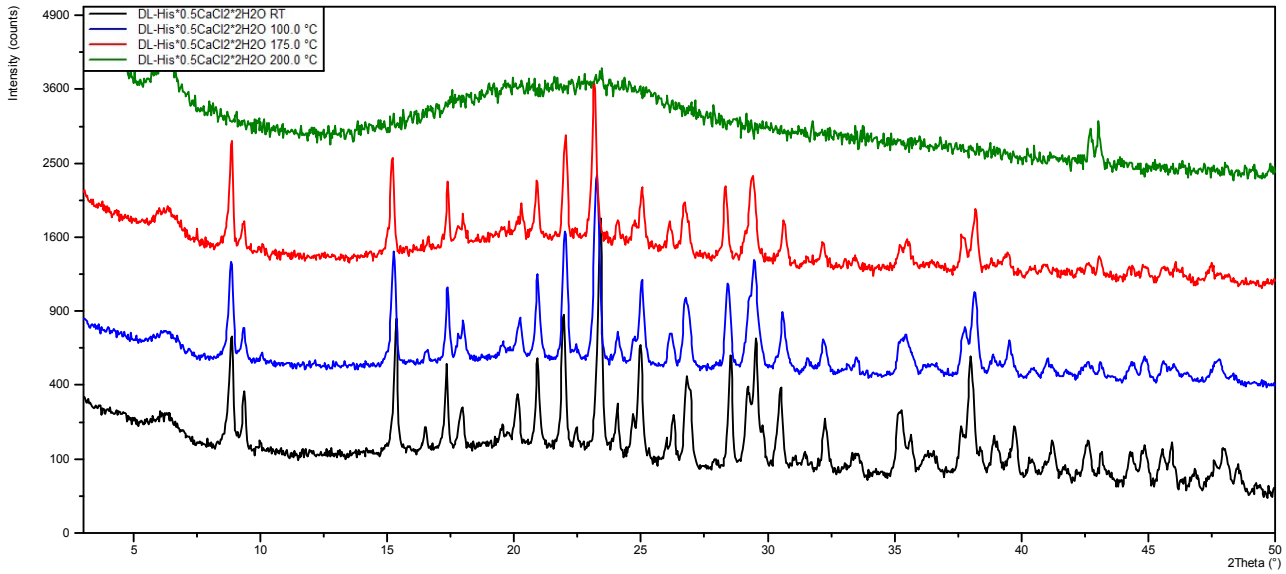

Figure ESI - 12. XRPD patterns of $(DL\text{-}His)_2{\cdot}CaCl_2{\cdot}3H_2O$ at room temperature, 100°C, 175 °C, 200 °C. The peaks at 43 ° 2θ are due to the sample holder.

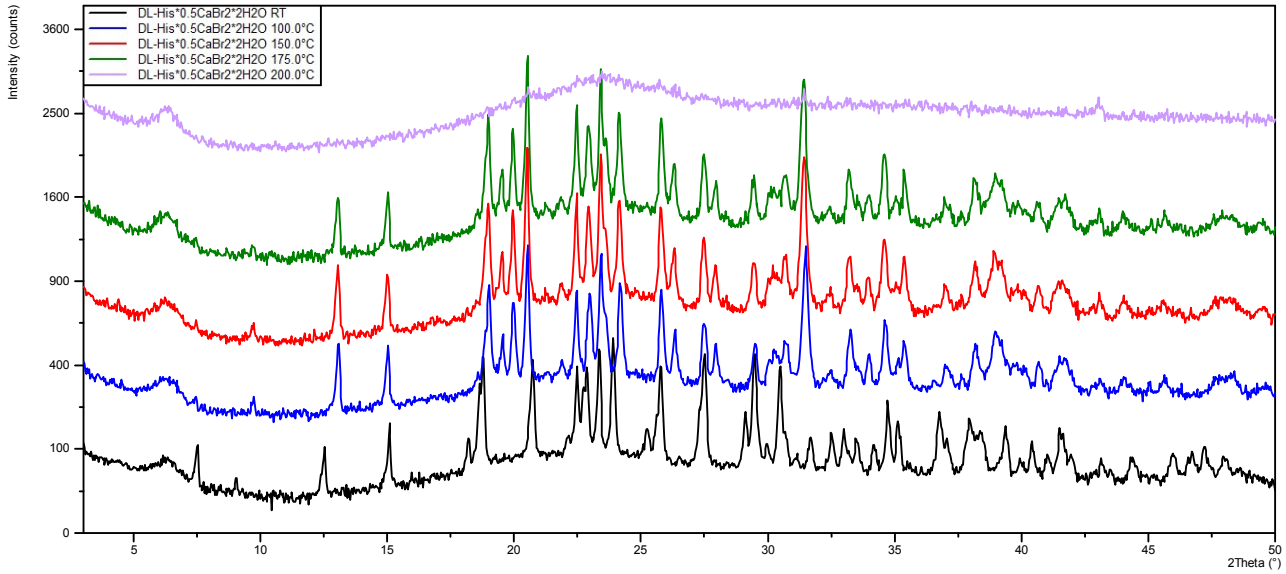

Figure ESI - 13. XRPD patterns of $(DL\text{-}His)_2{\cdot}CaBr_2{\cdot}4H_2O$ at room temperature, 100°C, 150 °C, 175 °C, 200 °C.

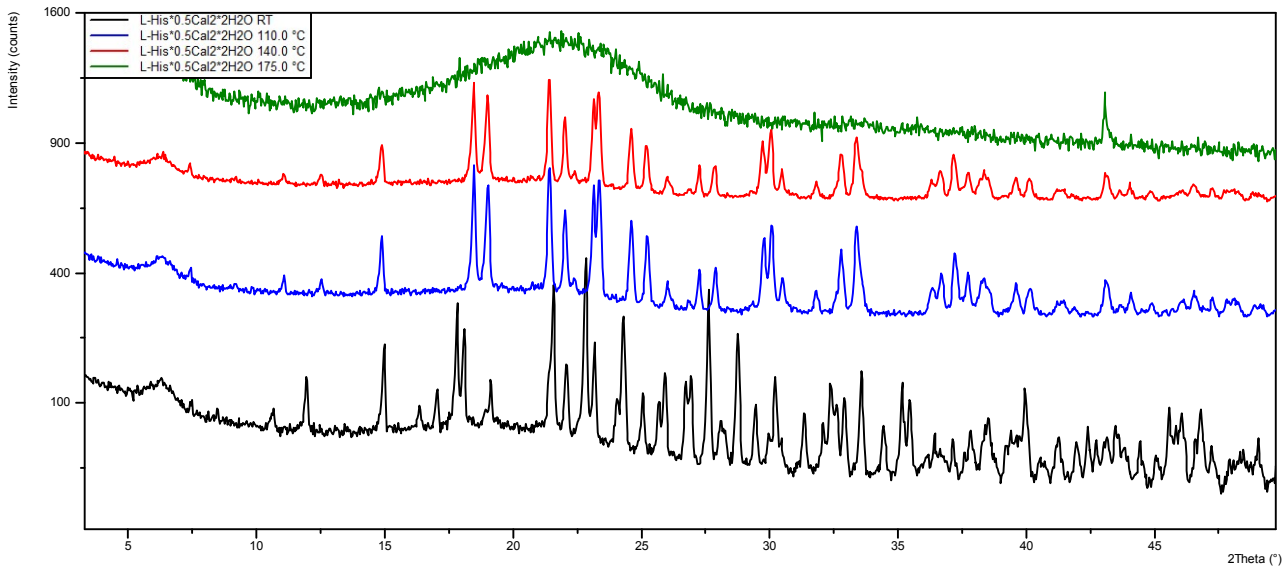

Figure ESI - 14. XRPD patterns of $(L\text{-}His)_2{\cdot}CaI_2{\cdot}4H_2O$ at room temperature, 100°C, 175 °C, 200 °C. The peaks at 43 ° 2θ are due to the sample holder.

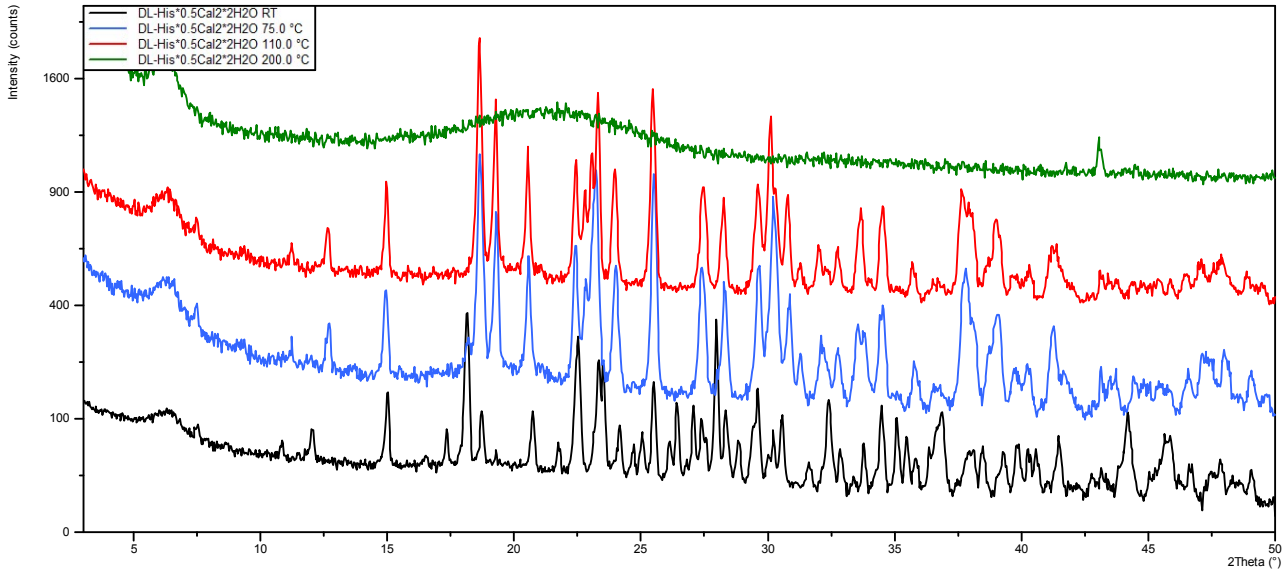

Figure ESI - 15. XRPD patterns of $(DL\text{-}His)_2{\cdot}CaI_2{\cdot}4H_2O$ at room temperature, 75°C, 110 °C, 200 °C. The peaks at 43 ° 2θ are due to the sample holder.

S5: Calculated and Experimental XRPD Patterns of $(L\text{-}His)_2{\cdot}CaI_2{\cdot}3H_2O$

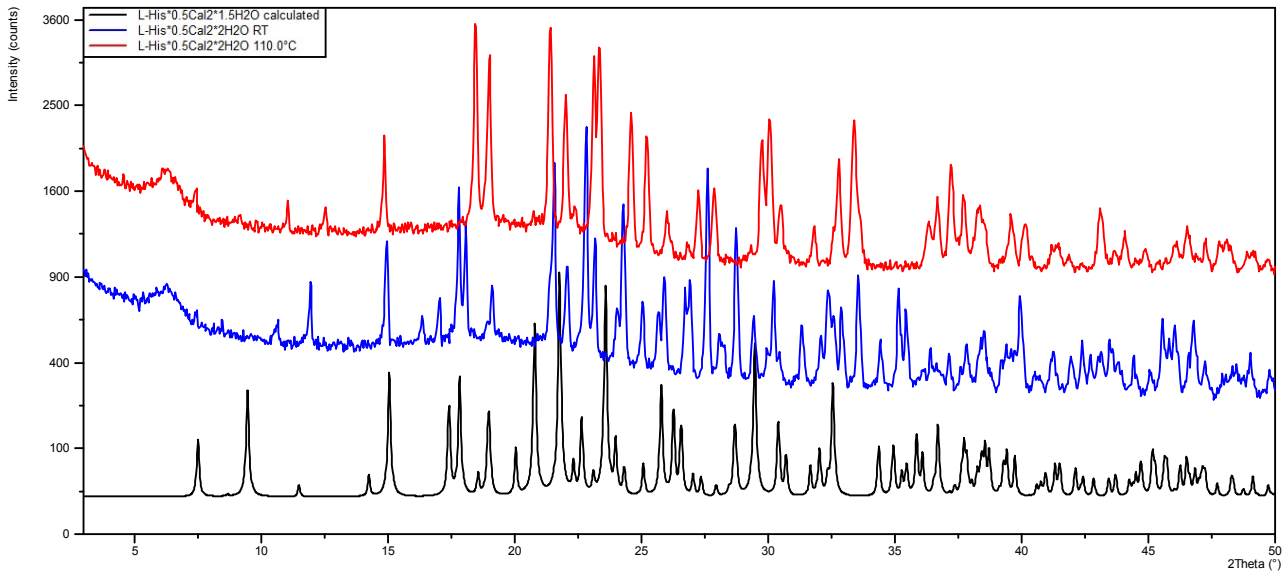

Figure ESI - 16. XRPD patterns of $(L\text{-}His)_2{\cdot}CaI_2{\cdot}4H_2O$ at room temperature and 110 °C compared to the calculated XRPD pattern of $(L\text{-}His)_2{\cdot}CaI_2{\cdot}3H_2O$.

ESI - 6: Structural determination of $(DL\text{-}His)_2{\cdot}CaCl_2{\cdot}3H_2O$, $(L\text{-}His)_2{\cdot}CaI_2{\cdot}4H_2O$ and $(DL\text{-}His)_2{\cdot}CaI_2{\cdot}4H_2O$

Laboratory data were used in the crystal structure determination. XRPD were analysed with the software X'Pert HighScore Plus[1] using DICVOL4 or DICVOL algorithms to find the right unit cell. $(DL\text{-}His)_2{\cdot}CaCl_2{\cdot}3H_2O$ was indexed in the monoclinic system, the structure was solved in the space group P $2_1/n$ by simulated annealing, performed with EXPO2014,[2] using Ca, Cl and O (as water: the precise position of hydrogen atoms of water molecules are difficult to establish using PXRD) atoms, and one molecule of histidine. Ten runs for simulated annealing trial were set, and a cooling rate (defined as the ratio Tn/Tn^{-1}) of 0.95 was used. The Rietveld refinement was subsequently performed with TOPAS 5.0[3] in the range 2θ=5-70.0°. The peak shape was modelled for size and strain with the Gaussian and Lorentzian functions present in TOPAS 5.0.

The refinement converged to R_{wp}=5.62 % and R_p= 4.22%.

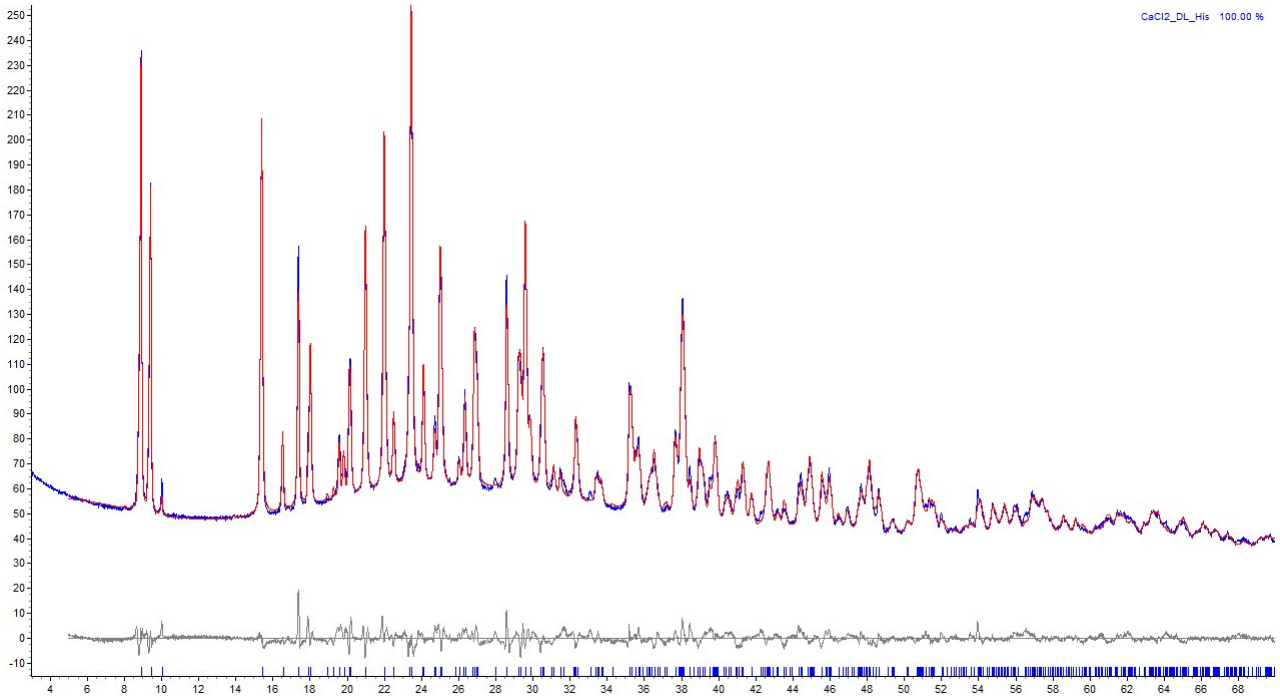

Figure ESI - 17. Rietveld analysis plot of $(DL\text{-}His)_2{\cdot}CaCl_2{\cdot}3H_2O$. Red line is the calculated diffractogram, blue line is the observed diffractogram and grey line is the difference plot. Y-axis is reported as $\sqrt{y}$.

The powder pattern of $(L\text{-}His)_2{\cdot}CaI_2{\cdot}4H_2O$ was indexed in the monoclinic system, space group I2, with a volume cell of 1206.16(3) $Å^3$ and a plausible solution was found with EXPO 2014 with the simulated annealing algorithm. Afterwards, it was used for Rietveld refinements in the range

2θ=5-70°, which were performed with the software TOPAS 5.0. The peak shape was modelled for size and strain with the Gaussian and Lorentzian functions present in TOPAS 5.0.

A small quantity (less than 1%) of $CaI_2 \cdot 8H_2O$ was identified in the product pattern, and its profile was refined on the basis of the known crystal structure.

The refinement converged to R_{wp}=4.40 % and R_p= 3.42%.

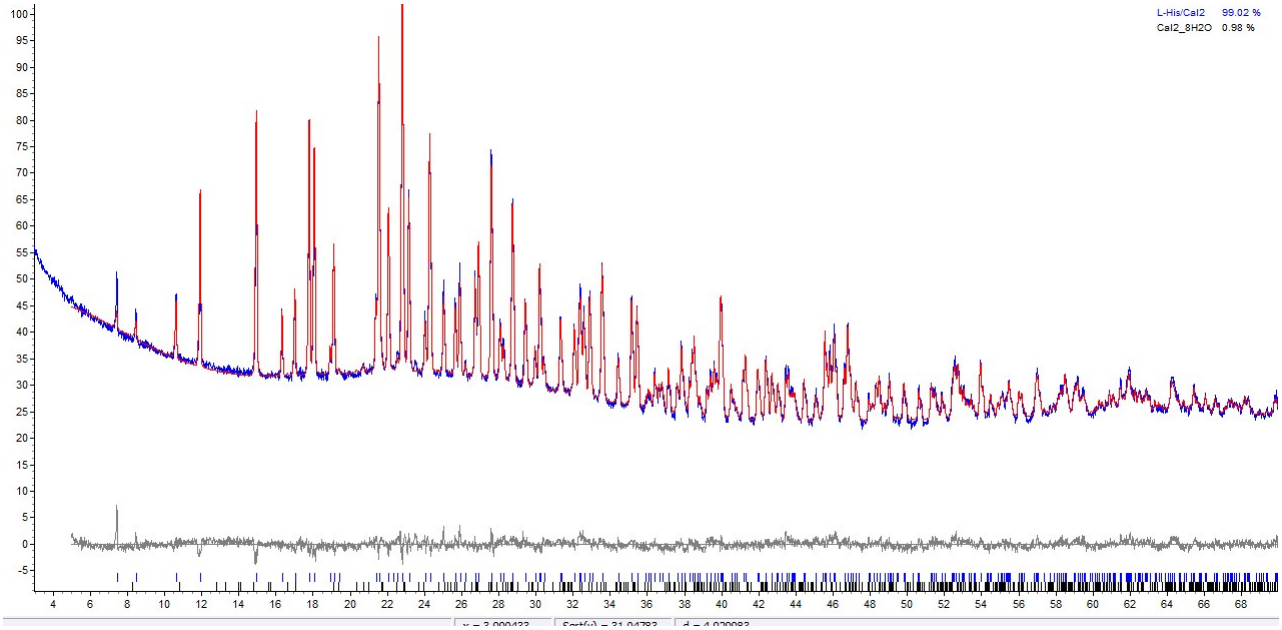

Figure ESI - 18. Rietveld analysis plot of $(L\text{-}His)_2 \cdot CaI_2 \cdot 4H_2O$. Red line is the calculated diffractogram, blue line is the observed diffractogram and grey line is the difference plot. Black and blue tick marks corresponds to of $(L\text{-}His)_2 \cdot CaI_2 \cdot 4H_2O$ and $CaI_2 \cdot 8H_2O$ l correspondingly. Y-axis is reported as $\sqrt{y}$.

The powder pattern of $(DL\text{-}His)_2 \cdot CaI_2 \cdot 4H_2O$ was indexed in the triclinic system, space group P-1. A plausible solution was found with EXPO 2014 with the simulated annealing algorithm and consequently used for Rietveld refinements performed with the software TOPAS 5.0. The peak shape was modelled for size and strain with the Gaussian and Lorentzian functions present in TOPAS 5.0.

A small quantity (less than 1%) of $CaI_2 \cdot 8H_2O$ was identified in the product pattern, and its profile was refined on the basis of the known crystal structure.

The refinement converged to R_{wp}= 4.35% and R_p= 3.30%.

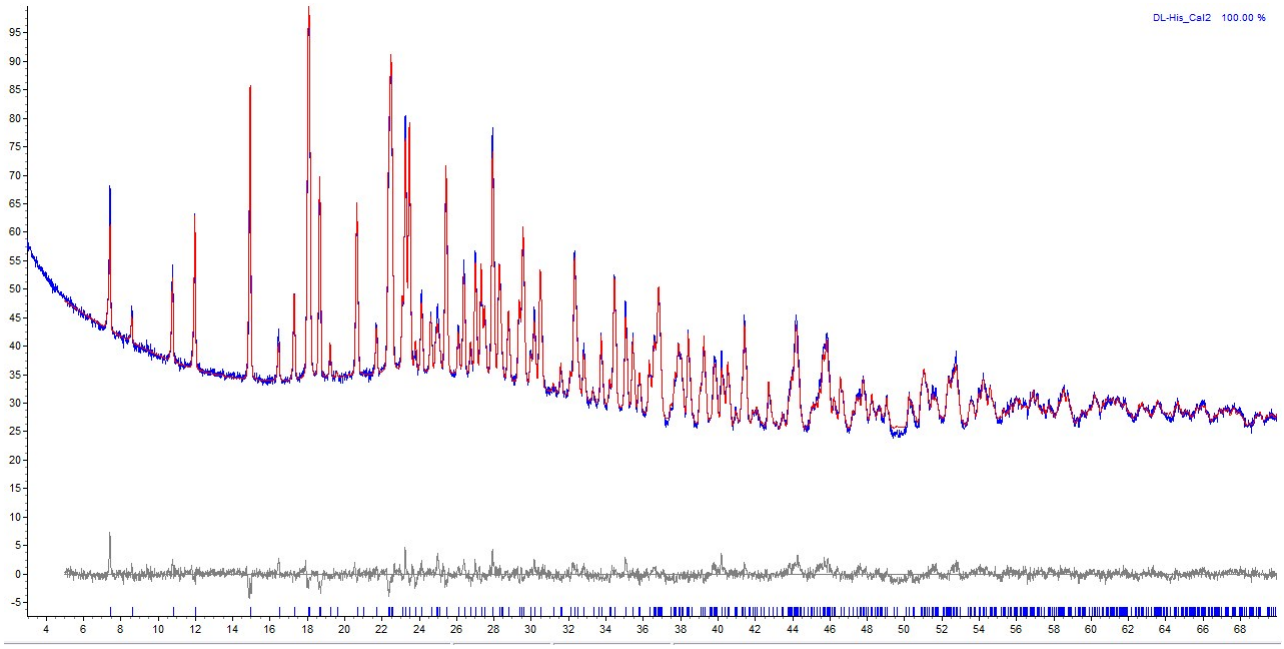

Figure ESI - 19. Rietveld analysis plot of $(DL\text{-}His)_2{\cdot}CaI_2{\cdot}4H_2O$. Red line is the calculated diffractogram, blue line is the observed diffractogram and grey line is the difference plot. Y-axis is reported as $\sqrt{y}$.

Structural data for the ICCs solved from XRPD are listed in Table S1.

Table ESI - 2. Structural data for $(DL\text{-}His)_2{\cdot}CaCl_2{\cdot}3H_2O$, $(L\text{-}His)_2{\cdot}CaI_2{\cdot}4H_2O$ and $(DL\text{-}His)_2{\cdot}CaI_2{\cdot}4H_2O$.

	$(DL\text{-}His)_2{\cdot}CaCl_2{\cdot}3H_2O$	**$(L\text{-}His)_2{\cdot}CaI_2{\cdot}4H_2O$**	**$(DL\text{-}His)_2{\cdot}CaI_2{\cdot}4H_2O$**
Formula	$C_{12}H_{24}N_6O_7Ca_1Cl_2$	$C_{12}H_{26}N_6O_8Ca_1I_2$	$C_{12}H_{26}N_6O_8Ca_1I_2$
Fw ($g*mol^{-1}$)	475.34	658.24	658.24
Crystal system	Monoclinic	Monoclinic	Triclinic
Space group	P $2_1/n$	I2	P-1
Z	4	4	2
a (Å)	18.878(4)	16.725(3)	4.9032(9)
b (Å)	5.0905(11)	4.8773(7)	10.5466(2)
c (Å)	10.799(3)	14.909(2)	11.965(3)
α (deg)	90.0	90	94.539(13)
β (deg)	97.857(13)	97.374(9)	95.925(13))
γ (deg)	90.0	90	102.71 (13)
V ($Å^3$)	1028.13(4)	1206.16(3)	597.06(2)
R_wp, %	5.62	4.40	4.35

References

1. Highscore Plus version 4.5. PANalytical B.V. 2016.

2. Altomare, A.; Cuocci, C.; Giacovazzo, C.; Moliterni, A.; Rizzi, R.; Corriero N.; Falcicchio, A. *J. Appl. Crystallogr.*, **2013**, 46, 1231–1235.

3. Cohelo, A., TOPAS-Academic, Coelho Software, Brisbane, Australia, **2007**.